Co3O4-decorated hematite nanorods as an effective photoanode for solar water oxidation

Xi, Lifei; Tran, Phong D.; Chiam, Sing Yang; Bassi, Prince Saurabh; Mak, Wai Fatt; Mulmudi, Hemant Kumar; Batabyal, Sudip Kumar; Barber, James; Loo, Say Chye Joachim; Wong, Lydia Helena

2012

Xi, L., Tran, P. D., Chiam, S. Y., Bassi, P. S., Mak, W. F., Mulmudi, H. K., et al. (2012). Co3O4-decorated hematite nanorods as an effective photoanode for solar water oxidation. Journal of physical chemistry C, 116(26), 13884-13889.

https://hdl.handle.net/10356/94973

https://doi.org/10.1021/jp304285r

Co_3O_4 decorated hematite nanorods as an effective photoanode for solar water oxidation

Lifei Xi [a], Phong D. Tran [b], Sing Yang Chiam [c], Prince Saurabh Bassi [a], Wai Fatt Mak [a], Hemant Kumar Mulmudi [b], Sudip K. Batabyal [b], James Barber [a,b,d,e], Joachim Say Chye Loo [a*], Lydia Helena Wong [a*]

[a] *School of Materials Science and Engineering, Nanyang Technology University, Singapore, 639798*

[b] *Energy Research Institute @ NTU, Nanyang Technological University, 50 Nanyang Drive, Research Techno Plaza, X-Frontier Block, Level 5, Singapore 637553*

[c] *Institute of Materials Research and Engineering(IMRE), Agency of Science, Technology, and Research (A* Star),3 Research Link, Singapore 117602, Singapore.*

[d] *Division of Molecular Biosciences Imperial College London, London, SW7 2AZ, UK*

[e] *BioSolar Laboratory, Department of Material Sciences and Chemical Engineering, Polytechnic of Torino, Corso Duca degli Abruzzi, 24, 10129, Torino, Italy*

* CORRESPONDING AUTHOR, E-mail: Joachimloo@ntu.edu.sg, Lydiawong@ntu.edu.sg

Abstract.

In this Article, we report a strategy to perform in situ incorporation of oxygen evolution catalyst, Co_3O_4, during hydrothermal growth of Fe_2O_3 nanorod arrays. It was found that the highest photocurrent increase and onset potential shift was observed with 5% Co^{2+}. The photocurrent density increases from 0.72 for the pristine Fe_2O_3 nanorod to 1.20 mA/cm^2 at 1.23 V versus RHE (i.e. 67 % improvement) with 5 % Co^{2+} added. Concomitant with this improvement was a shift in the onset potential by ~40 mV and improvements in incident-photo-to-current-efficiencies and oxygen evolution. Hematite photoanodes with in situ deposition of Co_3O_4 nanoparticles showed better performance than those prepared by ex situ procedures because of high surface roughness, larger Co_3O_4/hematite interfacial area and smaller Co_3O_4 particle size.

Keywords: Hematite, hydrothermal, in-situ, Co_3O_4, OEC, photoelectrochemical cells

Introduction

Photoelectrochemical (PEC) cells convert solar energy to stored chemical energy through the splitting of water into molecular oxygen and hydrogen. [1 - 3] Hematite (α-Fe_2O_3) has recently been extensively investigated as photoanode material for the generation of dioxygen from water due to its favorable optical band gap (E_g=2.2 eV), excellent chemical stability in aqueous environments, natural abundance and low cost. [4] Hematite has been theoretically predicted to achieve a water oxidation efficiency of 12.4%. [5] However, the reported efficiencies of hematite are lower than this predicted value, mainly due to the very short lifetime of photogenerated charge carriers (<10 ps), short hole diffusion length (2-4 nm), slow oxygen evolution reaction kinetics, low flat band potential and significant reduction in the absorption cross-section at wavelengths approaching the band gap value. [6] Another fundamental limitation of hematite system is the need for externally applied bias because the conduction band of hematite is lower than the potential required to reduce protons to hydrogen (in the vacuum scale).

Attempts to achieve higher efficiencies for hematite photoanodes include chemical composition modification by doping, manipulation of hematite nanostructures, surface modification with oxygen evolution catalysts (OEC), and surface passivation with inorganic materials. [4, 7] By adding impurities to act as electronic dopants, the conductive properties of hematite can be significantly enhanced.[4] Chemical modification of hematite by doping has been recently reviewed. [8, 9] The strategies to manipulate the dimensions and morphology of hematite on the nanometer scale include the deposition of porous thin films using solution-based colloidal methods, [10] growth of nanowire arrays on conducting substrates, [11] electrodeposition, [12] spray pyrolysis [13] and atmospheric pressure chemical vapor deposition (APCVD). [14] On the basis of the progress and limitations of all of the different approaches, the most promising candidates for achieving high efficiencies are those devices using nanowire or nanorod arrays because of the possibility of controlling the nanowire width to be within the hole diffusion length of hematite. [4] There are a number of methods to produce hematite nanowire array on substrates including thermal oxidation of iron foil, [15] the use of an anodic aluminum oxide (AAO) template,[16] and precipitation of Fe^{3+} from aqueous solution in hydrothermal conditions. [17, 18] Among these methods, hydrothermal precipitation of Fe^{3+} is the most simple and effective method. In a previous study [19], hematite nanorod arrays were successfully grown on conducting substrates by this method using urea as a pH-regulating agent. Well-aligned nanorods with an average

diameter of 90 nm and a length of 900 nm were produced. In comparison with other nanostructures, the nanorods showed better energy conversion efficiencies because of favorable [110] crystallographic orientation. However, because of the relatively large diameter (90 nm) of the nanorods, the conversion efficiency was not optimal. [19] A smaller diameter is required for charge transport so as to minimize the detrimental effect of the short diffusion length of holes and improve overall efficiency. [4, 6]

Surface modification with suitable catalyst (OEC) was also found to be an effective way to overcome kinetic issues of water oxidation by untreated hematite by, in part, acting as a charge storage system. Cobalt oxides have been extensively used as electrocatalysts for water oxidation applications when coated on surface of anodes. [20, 21] Cubic Co_3O_4 nanoparticles are much more active when the size is less than 5 nm. [21] For example, Jiao et al. found that nanosized Co_3O_4 particles in mesoporous silica (SMA-15) (4.2-8.6% w/w% loading) which was prepared by in-situ method can act as an effective water oxidation catalysts with the catalytic efficiency depending on the size of Co_3O_4 particles. [22, 23] Singh et al. reported microwave-assisted synthesis of Co_3O_4 on a Ni substrate. [24] This catalytic system showed a very high photocurrent density (100 mA/cm^2) in 1M KOH with an overpotential of 1.24V vs RHE. In addition, surface passivation with other inorganic materials, such as CoF_3, [25] Ga_2O_3 [26] and Al_2O_3, [27] has also shown improvements of photocurrent and lowering of offset potential.

In this work, we set out to produce Fe_2O_3/Co_3O_4 hybrids via hydrothermal methods. To the best of our knowledge, this is the first report describing the in-situ growth of cobalt oxides on the surface of hematite nanorod arrays. Unlike ex-situ growth of Co_3O_4 on hematite nanostructure, the advantages of our method include high Fe_2O_3/Co_3O_4 interfacial area induced by the hematite surface roughening and smaller Co_3O_4 particle size. The procedure developed is as follows: firstly, iron oxyhydroxide (FeOOH) was obtained from the reaction of $FeCl_3$ and urea in an aqueous solution at 100 °C (see Supporting Information). FeOOH nanorod arrays were successfully grown on FTO substrates after heating inside an autoclave for 8 hrs. Secondly, FeOOH nanorods were converted to hematite during annealing at 550 °C for 2 hr. These nanorod arrays were further annealed at 800 °C for 20 min. When Co^{2+} was added initially, FeOOH nanorods were decorated with cobalt oxyhydroxide (CoOOH) which were converted to Co_3O_4

particles during annealing. In this study, we found that the photocurrent and onset potential of Co_3O_4 decorated hematite photoanodes showed significant improvement compared to that of pristine hematite.

Results and Discussion

The top view SEM image of the FeOOH nanorods is shown in Fig. 1a, and the nanorods were found to be square in cross-section. After annealing at 550 °C for 2 hr, the film color changed from yellow to dark red, suggesting successful conversion from FeOOH to hematite. [6] The morphology of these square nanorods also changed (see Fig 1b). The sharp edge of square rods disappeared and became rounded. The average rod length after annealing at 550 °C for 2 hr was about 380 nm and the diameter was 60 nm (see Fig 1b inset). After further annealing of the film at 800 °C for 20 min, its color changed to light red. This resulted in an increase in diameter to about 80 nm which was probably due to aggregation at high temperature annealing (see Fig 1c). This increase in diameter could be undesirable because it may lead to a reduction in conductivity and a disordered morphology of FTO substrates. [6] However, some studies have shown that high temperature annealing can induce the diffusion of Sn from the FTO layer into the hematite with a consequential increase in conductivity. [6, 10] Thus, in order to achieve a better performance, all these parameters have to be considered and optimized. In this study, we found that annealing at 800 °C for 20 min is an optimization procedure based on the performance of the system, a result which is consistent with previous reports. [6, 7, 10, 28]

TEM images of pristine hematite nanorods and those with Co^{2+} added during hematite growth are shown in Fig 2a-b. Introducing Co^{2+} ions was found to change the morphology drastically which is in agreement with previous studies. [6, 28] The surface of the untreated hematite nanorods was smooth while the surface of nanorods with Co^{2+} was rougher (see Fig 2a-b). The reason for roughening of hematite could be due to the presence of nitrate anions which come from $Co(NO_3)_2$ in the reaction solution. These nitrate anions may accelerate the phase transformation from previously formed FeOOH to Fe_2O_3 via dissolution, thus result in a roughen surface of FeOOH. [29] A rough surface is preferred because it increases the surface area of rods, and thus leads to improvements in charge separation and transport to the semiconductor/electrolyte interface. [4] Fig 2c shows HRTEM image of the region marked in Fig 2b. Black dots, with

average diameters of ~4nm and indexed to cubic Co_3O_4 (JCPDS #042-1467), are observed on the surface of a hematite rod. On the other hand ex-situ growth of Co_3O_4 on the surface of hematite nanorod arrays show a smooth surface and larger Co_3O_4 particles (few tens nanometer) (see Fig 2d and Fig S1). The XRD pattern of nanorod film after 8 hr reaction can be indexed to the characteristic peaks of FeOOH (JCPDS #003-0440) (see Fig 3a). After annealing at 550 °C for 2 hr, the absence of FeOOH diffraction peaks confirms the complete conversion of FeOOH to hematite. Strong (110) diffraction peak at $2\theta = 35.8$ ° implies hematite nanorods growth orientation is [110]. [4, 6, 7] This is preferred because the conductivity in the basal plane (001) is up to 4 orders of magnitude higher than the orthogonal plane which facilitates the charge transport and collection during the photo-oxidation process. When Co^{2+} is added with an initial molar ratio of Co^{2+} to Fe^{3+} of 5%, there is neither a peak shift nor broadening of XRD peaks, which is normally associated with doping or solid solution formation. The absence of Co_3O_4-induced effect on the XRD pattern could imply that the quantity of Co incorporated with the hematite nanorods might be too small to be detected. However, XPS and EDAX spectra of hematite confirmed the presence of Co (see Fig. 3b and Fig S2-3). From XPS spectra, the Co 3s scan has two peaks at 101.62 and 102.6 eV, which correspond to Co^{II} and Co^{III} of Co_3O_4. [30] Based on the Co 3s signal, the Co content on the surface of hematite nanorods is substantial and the molar ratio of Co-to-Fe is estimated to be around 8%. Since this ratio is higher than the initial value (5 % Co^{2+} added), we can deduce that Co is mainly dispersed on the surface of hematite nanorods. In addition, the survey scans show no detectable Cl (Cl $2p^{3/2}$ at 198.5 eV) and F (F 1s at 685 eV) ions in both the pristine hematite and hematite decorated with Co_3O_4 (see Fig S2) which is sufficient to confirm that no Cl anions remain in the samples and F ions diffused from FTO are negligible. UV-Vis spectra of samples with and without Co^{2+} added at a molar ratio of 5% are shown in Fig. 4a. It can be seen that the shape of the absorption curves and the Tauc-Plots fitted bandgaps are nearly the same (Fig. 4b). The reason of smaller bandgaps for both samples compared to that of reported (2.04 eV) [28] is probably due to minor Sn diffusion (doping) from FTO. Several studies have confirmed experimentally that high temperature annealing can introduce Sn from FTO. [6, 10, 28] The absorption of films from 450 to 750 nm is enhanced mainly because of the rough surface of hematite (see Fig 4a inset for the pure Co_3O_4 absorption) rather than due to the absorption of Co_3O_4 particles which have typical absorption from 600 to 850 nm. [31] The similar bandgap values also imply that Co doping has not occurred.

Fig. 5a shows photocurrent-potential curves of pristine hematite and hematite with different amount of Co^{2+} added. It was found that the addition of Co^{2+} gave rise to a strong effect on the photocurrent-potential characteristics. The photocurrent density increased from 0.72 for the untreated hematite nanorods to 0.84, 0.96 and 1.20 mA/cm^2 with 0.1, 1 and 5 % Co^{2+} added respectively. In this study, all potentials mentioned were referred to a reversible hydrogen electrode (RHE). With an initial onset potential of 0.66 V in 1 M (pH=13.6) NaOH electrolyte, the photo-induced current density generated by the hematite photoanode with 5 % Co^{2+} increased rapidly, attaining approximately 1.2 mA/cm^2 at 1.23 V and reached a plateau of about 1.8 mA/cm^2 at 1.4 - 1.6 V before the current increased exponentially. The photocurrent of hematite photoanode with 5 % Co^{2+} added at 1.23 V increased 67% compared to the pristine hematite nanorods. Note, that the photocurrent density at 1.23V with 5 % Co^{2+} added is much higher than other OEC modified hematite photoanodes, including those treated with CoF_3, [25] Ga_2O_3, [26] Co-Pi [7, 32 - 35] and Ni-Bi [7]. The enhancement of the photocurrent can be attributed to the catalytic effect of the Co_3O_4 nanoparticles as well as increased absorption (see Fig 4a). Despite that high temperature annealing can make Sn diffusion from FTO as mentioned above, this should not be the dominant effect for the photocurrent improvement in this study. It is because both the pristine hematite and hematite with 5 % Co^{2+} added were annealed under these conditions. Further increasing Co^{2+} level to 10 % or higher resulted in a decrease of photocurrent which was probably due to the formation of more Co_3O_4 particles on the surface of hematite nanorods, which may block the hole transport to the interface. Another possible reason is that a substantial morphology change occurs due to more Co^{2+} ions introduced in the course of hydrothermal reaction. [6, 28] Thus, 5% Co^{2+} addition was found to be the optimal amount in this study. Interestingly, a positive shift of onset potential was also observed for hematite with 0.1, 1 and 5 % Co^{2+} added. The highest onset potential shift obtained with 5 % Co^{2+} was around 40 mV.

It is worth emphasizing that hematite photoanodes with in-situ deposition of Co_3O_4 nanoparticles showed the best performance compared to ex-situ growth procedures (see Fig 5b). The reasons for the poor performance for these ex-situ procedures are probably due to a reduced roughness of hematite nanorods and the bigger size of Co_3O_4 particles as compared to ~4 nm of in-situ Co_3O_4 nanoparticles (see Fig 2d). To conclude, it seems that the benefit of in-situ growth of Co_3O_4

particles on hematite is the generation of nanosized Co_3O_4 particles and large Co_3O_4/hematite interfacial area which results in improved photocatalytic properties. This conclusion is consistent with that of Jiao et al. [22], whereby they observed that the oxygen yield from the in-situ grown nanosized Co_3O_4 clusters in mesoporous silica (4%) was 1550 times higher than that of bare micrometer-sized Co_3O_4 particles. They also found that samples with smaller Co_3O_4 clusters size can generate 1.5 times more oxygen gas than that of bigger ones due to a larger surface area. The photocurrent improved was further verified by measuring the photoanode incident-photo-to-current-efficiencies (IPCE) at 1.23 V as a function of incident light wavelength (see Fig 6). It can be seen that the hematite decorated with 5% Co^{2+} showed substantially enhanced IPCE values compared to the pristine hematite, which are consistent with their photocurrent-potential characteristics. The IPCE drops to zero at wavelengths longer than 610 nm, which is consistent with the energetics of the hematite band gap.[6]

In order to study the reason of onset potential shift with increasing Co levels up to 5%, electrochemical impedance spectroscopy (EIS) measurements were carried out. Mott-Schottky analysis shows that the flat-band potential of the sample shifted by -50 mV when Co^{2+} was added (see Fig 7). The reason of flat-band potential shift is probably due to the efficient hole transport from hematite to Co_3O_4, thus changing the band alignment. This result is consistent with the photocurrent-potential data (Fig 5a), where a negative shift of 40 mV with respect to pristine hematite was observed for the sample with 5% Co^{2+} added. Finally, the oxygen generation was recorded by gas chromatography as shown in Fig 8. It can be seen that the amount of oxygen generated with Co 5% decorated hematite photoanode was stable and larger than that of the pristine. The Faradaic efficiencies of both the pristine hematite and hematite decorated with 5% Co^{2+} were calculated and equal to 69.46 and 78.43% which indicates that the amount of O_2 evolved is less than that of expected. It is probably because O_2 evolved was partially remained in the initially degassed NaOH solution and also because of gas leakage during manual injection.

Conclusions

In summary, we combined hydrothermal method for Fe_2O_3 nanorod arrays and in-situ growth of Co_3O_4 nanoparticles to achieve higher photocurrent and lower onset potential for light-induced water oxidation compared to untreated Fe_2O_3. The effect of Co^{2+} concentration on the PEC cell

performance was also studied and found that 5% Co^{2+} addition shows the highest photocurrent increase and onset potential shift. With this level of added Co, the photocurrent density increased from 0.72 for the pristine Fe_2O_3 nanorods to 1.20 mA/cm^2 at 1.23 V *vs* RHE (i.e. 67 % improvement) and the onset potential shifted by about 40 mV. Concomitant with this was improvements in IPCE and oxygen evolution. It was also found that hematite photoanodes with in-situ deposition of Co_3O_4 nanoparticles showed better performance than those prepared by other ex-situ growth procedures, most probably because of surface roughness and smaller Co_3O_4 particle size.

Supporting information

Full experiment details and the additional figures. This materials is available free of charge via the Internet at http://pubs.acs.org.

Acknowledgment

Financial supports from the Centre of Artificial Photosynthesis and MOE Tier 1 are gratefully acknowledged.

References

1. Fujishima, A.; Honda, K. *Nature* **1972**, *238*, 37.

2. Khaselev, O.; Turner, J. A. *Science* **1998**, *280*, 425.

3. Gratzel, M. *Nature* **2001**, *414*, 338.

4. Sivula, K.; Le Formal, F.; Gratzel, M. *ChemsusChem* **2011**, *4*, 432.

5. Murphy, A. B.; Barnes, P. R. F.; Randeniya, L. K.; Plumb, I. C.; Grey, I. E.; Horne, M. D.; Glasscock, J. A. *Int. J. Hydrogen Energy* **2006**, *31*, 1999.

6. Ling, Y.; Wang, G.; Wheeler, D. A.; Zhang, J. Z.; Li, Y. *Nano Lett.* **2011**, *11*, 2119.

7. Hong, Y. R.; Liu, Z. L.; Al-Bukhari, S. F. B. S. A.; Lee, C. J. J.; Yung, D. L.; Chi, D. Z.; Hor. T. S. A. *Chem. Commun.* **2011**, *47*, 10653.

8. Shinar, R.; Kennedy, J. H. *Sol. Energy Mater.* **1982**, *6*, 323.

9. Liao, P.; Toroker, M. C.; Carter, E. A. *Nano Lett.* **2011**, *11*, 1775.

10. Sivula, K.; Zboril, R.; Le Formal, F.; Robert, R.; Weidenkaff, A.; Tucek, J.; Frydrych, J.; Gratzel, M. *J. Am. Chem. Soc.* **2010**, *132*, 7436.

11. Beermann, N.; Vayssieres, L.; Lindquist, S. E.; Hagfeldt, A. *J. Electrochem. Soc.* **2000**, *147*, 2456.

12. Hu, Y. S.; Kleiman-Shwarsctein, A.; Forman, A. J.; Hazen, D.; Park J. N.; McFarland, E. W.; *Chem. Mater*. **2008**, *20*, 3803.

13. Murthy, A. S. N.; Reddy, K. S. *Mater. Res. Bull.* **1984**, *19*, 241.

14. Tilley, S.; Cornuz, M.; Sivula, K.; Gratzel, M. *Angew. Chem. Int. Ed.* **2010**, *49*, 6405.

15. Fu, Y. Y.; Wang, R. M.; Xu, J.; Chen, J.; Yan, Y.; Narlikar, A. V.; Zhang, H. *Chem. Phys. Lett.* **2003**, *379*, 373.

16. Mohapatra, S. K.; John, S. E.; Banerjee, S.; Misra, M. *Chem. Mater.* **2009**, *21*, 3048.

17. Vayssieres, L.; Beermann, N.; Lindquist, S. E.; Hagfeldt, A. *Chem. Mater.* **2001**, *13*, 233.

18. Peng, L. L.; Xie, T. F.; Fan, Z. Y.; Zhao, Q. D.; Wang, D. J.; Zheng, D. *Chem. Phys. Lett.* **2008**, *459*, 159.

19. Mulmudi, H. K.; Mathews, N.; Dou, X. C.; Xi, L. F.; Pramana, S. S.; Lam, Y. M.; Mhaisalkar, S. G. *Electrochem. Commun.* **2011**, *13*, 951.

20. Elizarova, G. L.; Zhidomirov, G. M.; Parmon, V. N. *Catal. Today* **2000**, *58*, 71.

21. Artero, V.; Chavarot-Kerlidou, M.; Fontecave, M. *Angew. Chem., Int. Ed.* **2011**, *50*, 7238.

22. Jiao, F.; Frei, H. *Angew. Chem. Int. Ed.* **2009**, *48*, 1841.

23. Jiao, F.; Frei, H. *Chem. Comm.* **2010**, *46*, 2920.

24. Singh, R. N.; Mishra, D.; Anindita; Sinha, A. S. K.; Singh, A. *Electrochem. Commun.* **2007**, *9*, 1369.

25. Hu, Y. S.; Kleiman-Shwarsctein, A.; Stucky G. D.; McFarland, E. W. *Chem. Commun.* **2009**, 2652.

26. Hisatomi, T.; Le Formal, F.; Cornuz, M.; Brillet, J.; Tetreault, N.; Sivula, K.; Gratzel, M. *Energy Environ. Sci.* **2011**, *4*, 2512.

27. Le Formal, F.; Tetreault, N.; Cornuz, M.; Modehl, T.; Gratzel, M.; Sivula, K. *Chem. Sci.* **2011**, *2*, 737.

28. Qin, D. D.; Tao, C. L.; In, S. I.; Yang, Z. Y.; Mallouk, T. E.; Bao, N. Z.; Grimes, C. A. *Energy Fuels* **2011**, *25*, 5257.

29. Music, S.; Maljkovic, M.; Czako-Nagy, I. *Mater. Lett.* 1997, 31, 43.

30. Greenwood, N. N.; Earnshaw, A. *Chemistry of the Elements (2nd ed.).* Butterworth-Heinemann: Oxford, U.K., 1997; p 804.

31. Long, M. C.; Cai, W. M.; Cai, J.; Zhou, B. X.; Chai, X. Y.; Wu, Y. H. *J. Phys. Chem. B* **2006**, *110*, 20211.

32. Zhong, D. K.; Sun, J. W.; Inumaru, H.; Gamelin, D. R. *J. Am. Chem. Soc.* **2009**, *131*, 6086.

33. Zhong D. K.; Gamelin, D. R. *J. Am. Chem. Soc.* **2010**, *132*, 4202.

34. McDonald, K. J.; Choi, K. S. *Chem. Mater.* **2011**, *23*, 1686.

35. Barroso, M.; Cowan, A. J.; Pendlebury, S. R.; Gratzel, M.; Klug, D. R.; Durrant, J. R. *J. Am. Chem. Soc.* **2011**, *133*, 14868.

Figures and captions

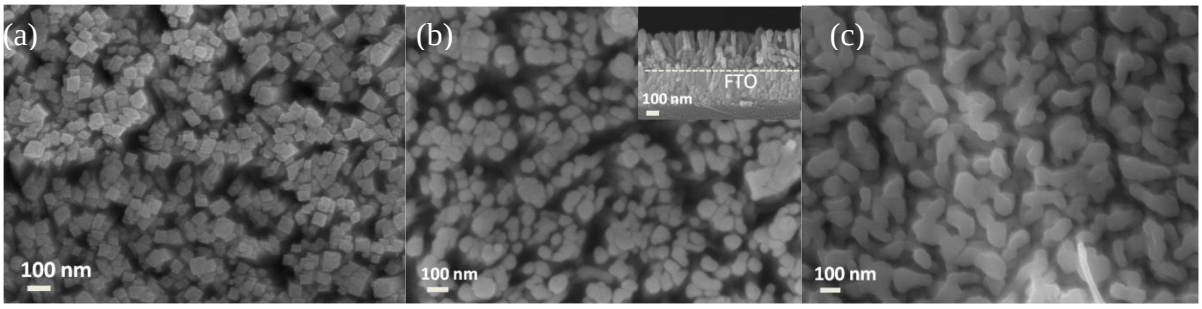

Fig. 1 SEM image of (a) FeOOH, (b) hematite after annealing at 550°C for 2 h (inset: cross-section image) and (c) hematite after additional annealing at 800°C for 20 min of hematite nanorod array.

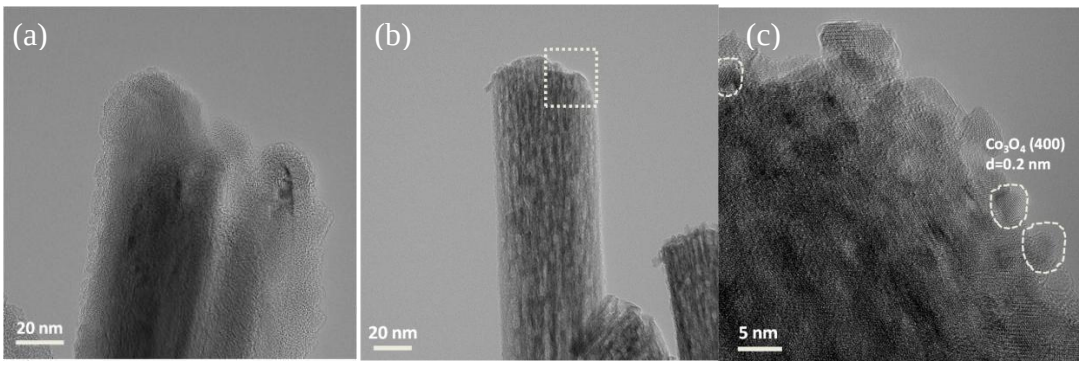

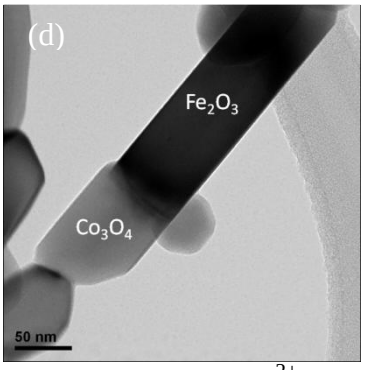

Fig. 2 TEM image of hematite nanorods (a) without Co^{2+} added, (b) with 5% Co^{2+} added and (c) HRTEM image of the region marked in image (b). All these samples were annealed at 550 °C for 2 h. (d) TEM image of ex situ hydrothermal growth of FeOOH nanorod arrays, followed by hydrothermal growth of CoOOH.

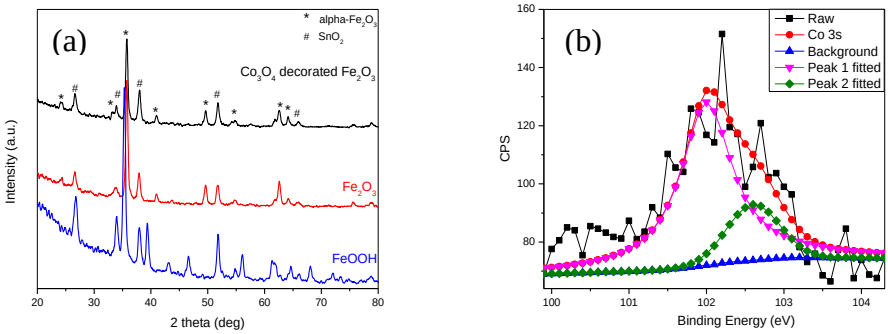

Fig. 3 (a) XRD patterns of hematite nanorod arrays on FTO without and with Co_3O_4 decorated after annealing at 550 °C for 2 h. Note: The molar ratio of Co^{2+} to Fe^{3+} is equal to 5% for Co_3O_4 decorated sample. The * denotes Fe_2O_3 (JCPDS 33-0664) and # denotes SnO_2 (JCPDS 46-1088), respectively. (b) XPS spectra of Co 3s scan.

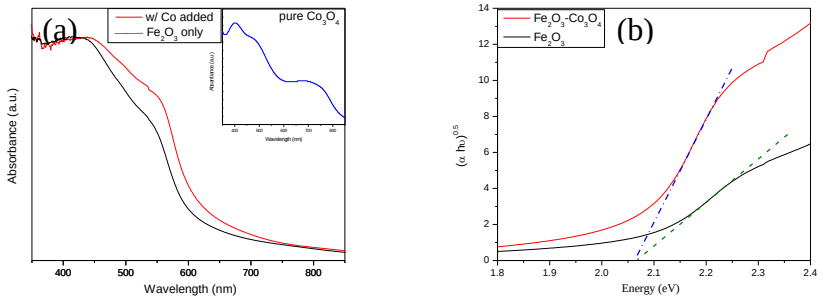

Fig. 4 (a) UV-Vis absorption (inset: pristine Co_3O_4 absorption) and (b) Tauc-Plots of films of hematite with and without Co_3O_4 decorated.

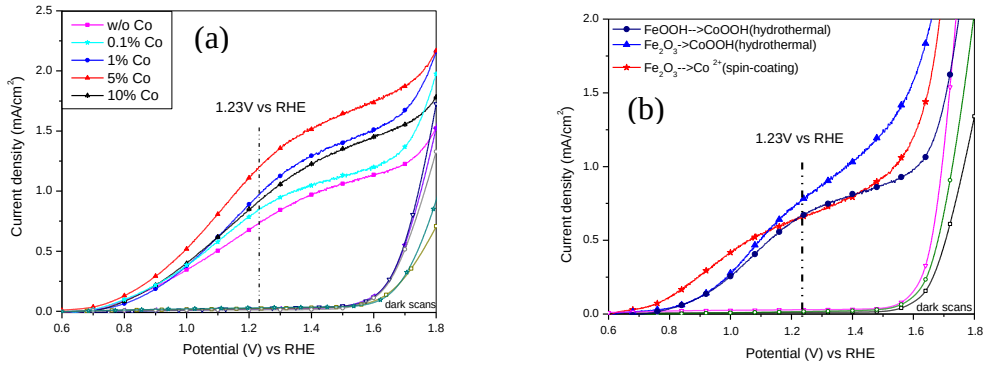

Fig. 5 Photocurrent-potential curves of hematite photoanode: (a) with different amount of Co^{2+} added in situ and (b) prepared by ex-situ growths: FeOOH → CoOOH (hydrothermal), Fe_2O_3 → CoOOH (hydrothermal), and Fe_2O_3→Co^{2+} (spin-coating).

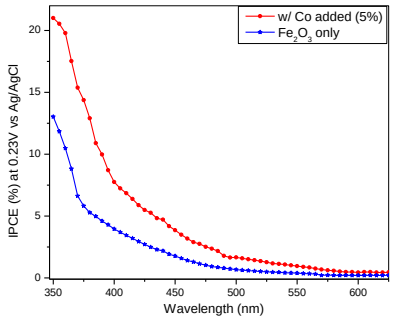

Fig. 6 IPCE spectra of hematite with and without 5% Co added at an applied potential of 1.23 V *vs* RHE in a 1 M NaOH electrolyte.

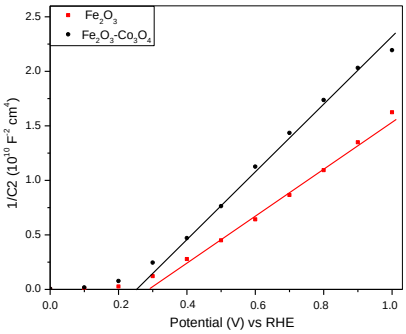

Fig. 7 Mott-Schottky plots of hematite films, hematite films with Co_3O_4 decorated tested in a 1 M NaOH electrolyte (pH 13.6) in the dark.

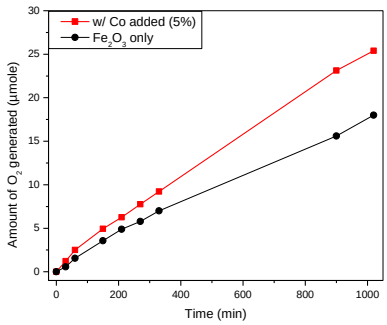

Fig. 8 Time course of oxygen evolution of hematite photoanodes with and without 5% Co added at an applied potential of 1.23 V versus RHE in a 1 M NaOH electrolyte based on equal levels of hematite.